

Mixing angles and electromagnetic properties of ground state pseudoscalar and vector meson nonets in the light-cone quark model

Ho-Meoyng Choi and Chueng-Ryong Ji

Department of Physics, North Carolina State University, Raleigh, N.C. 27695-8202

Abstract

Both the mass spectra and the wave functions of the light pseudoscalar (π, K, η, η') and vector(ρ, K^*, ω, ϕ) mesons are analyzed within the framework of the light-cone constituent quark model. A gaussian radial wave function is used as a trial function of the variational principle for a QCD motivated Hamiltonian which includes not only the Coulomb plus harmonic oscillator potential but also the hyperfine interaction to obtain the correct $\rho - \pi$ splitting. The mixing angles of $\omega - \phi$ and $\eta - \eta'$ are predicted and various physical observables such as decay constants, charge radii, and radiative decay rates *etc.* are calculated. Our numerical results are in a good agreement with the available experimental data.

12.39.Ki,13.40.Gp,13.40.Hq,14.40.-n

I. INTRODUCTION

It has been realized that the relativistic effects are crucial to describe the low-lying hadrons made of u, d and s quarks and anti-quarks [1]. The light-cone quark model [2–12] takes the advantages of the equal light-cone time($\tau = t + z/c$) quantization and includes the important relativistic effects in the hadronic wave functions. The distinct features of the light-cone equal- τ quantization compared to the ordinary equal- t quantization may be summarized as the suppression of vacuum fluctuations with the decoupling of complicated zero-modes and the conversion of the dynamical problem from boost to rotation.

The suppression of vacuum fluctuations is due to the rational energy-momentum dispersion relation which correlates the signs of the light-cone energy $k^- = k^0 - k^3$ and the light-cone momentum $k^+ = k^0 + k^3$ [5]. However, the non-trivial vacuum phenomena can still be realized in the light-cone quantization approach if one takes into account the non-trivial zero-mode($k^+ = 0$) contributions. As an example, it is shown [13] that the axial anomaly in the Schwinger model can be obtained in the light-cone quantization approach by carefully analyzing the contributions from zero-modes. Therefore, in the light-cone quantization approach, one can take advantage of the rational energy-momentum dispersion relation and build a clean Fock state expansion of hadronic wave functions based on a simple vacuum by decoupling the complicated non-trivial zero-modes. The decoupling of zero-modes can be achieved in the light-cone quark model since the constituent quark and anti-quark acquire appreciable constituent masses. Furthermore, the recent lattice QCD results [14] indicated that the mass difference between η' and pseudoscalar octet mesons due to the complicated nontrivial vacuum effect increases(or decreases) as the quark mass m_q decreases(or increases), *i.e.*, the effect of the topological charge contribution should be small as m_q increases. This supports us to build the constituent quark model in the light-cone quantization approach because the complicated nontrivial vacuum effect in QCD can be traded off by the rather large constituent quark masses. One can also provide a well-established formulation of various form factor calculations in the light-cone quantization method using the well-known Drell-Yan-West($q^+ = 0$) frame. We take this as a distinctive advantage of the light-cone quark model.

The conversion of the dynamical problem from boost to rotation can also be regarded as an advantage because the rotation is compact, *i.e.*, closed and periodic. The reason why the rotation is a dynamical problem in the light-cone quantization approach is because the

quantization surface $\tau = 0$ is not invariant under the transverse rotation whose direction is perpendicular to the direction of the quantization axis z at equal τ [15]. Thus, the transverse angular momentum operator involves the interaction that changes the particle number and it is not easy to specify the total angular momentum of a particular hadronic state. Also τ is not invariant under parity [16]. We circumvent these problems of assigning the quantum numbers J^{PC} to hadrons by using the Melosh transformation of each constituents from equal t to equal τ .

In our light-cone quark model of mesons, the meson state $|M\rangle$ is thus represented by

$$|M\rangle = \Psi_{Q\bar{Q}}^M |Q\bar{Q}\rangle, \quad (1.1)$$

where Q and \bar{Q} are the effective dressed quark and anti-quark. The model wave function is given by

$$\Psi_{Q\bar{Q}}^M = \Psi(x, \mathbf{k}_\perp, \lambda_q, \lambda_{\bar{q}}) = \sqrt{\mathcal{J}} \phi(x, \mathbf{k}_\perp) \mathcal{R}(x, \mathbf{k}_\perp, \lambda_q, \lambda_{\bar{q}}), \quad (1.2)$$

where $\phi(x, \mathbf{k}_\perp)$ is the radial wave function, \mathcal{J} is a Jacobi factor and $\mathcal{R}(x, \mathbf{k}_\perp, \lambda_q, \lambda_{\bar{q}})$ is the spin-orbit wave function obtained by the interaction-independent Melosh transformation. When the longitudinal component k_n is defined by $k_n = (x - 1/2)M_0 + (m_q^2 - m_{\bar{q}}^2)/2M_0$, the Jacobian of the variable transformation $\{x, \mathbf{k}_\perp\} \rightarrow \mathbf{k} = (k_n, \mathbf{k}_\perp)$ is given by

$$\mathcal{J} = \frac{\partial k_n}{\partial x} = \frac{M_0}{4x(1-x)} \left\{ 1 - \left[\frac{(m_{\bar{q}}^2 - m_q^2)}{M_0^2} \right]^2 \right\}. \quad (1.3)$$

The explicit spin-orbit wave function of definite spin (S, S_z) can be obtained by

$$\begin{aligned} \mathcal{R}(x, \mathbf{k}_\perp, \lambda_q \lambda_{\bar{q}}) &= \sum_{s_q, s_{\bar{q}}} \langle \lambda_q | \mathcal{R}_M^\dagger(x, \mathbf{k}_\perp, m_q) | s_q \rangle \\ &\quad \times \langle \lambda_{\bar{q}} | \mathcal{R}_M^\dagger(1-x, -\mathbf{k}_\perp, m_{\bar{q}}) | s_{\bar{q}} \rangle \langle \frac{1}{2} s_q \frac{1}{2} s_{\bar{q}} | S S_z \rangle, \end{aligned} \quad (1.4)$$

where the Melosh transformation is given by

$$\mathcal{R}_M(x, \mathbf{k}_\perp, m) = \frac{m + xM_0 - i\sigma \cdot (\hat{\mathbf{n}} \times \hat{\mathbf{k}})}{\sqrt{(m + xM_0)^2 + \mathbf{k}_\perp^2}} \quad (1.5)$$

with $\hat{\mathbf{n}} = (0, 0, 1)$ being a unit vector in the z -direction.

While the spin-orbit wave function is in principle uniquely determined by the Melosh transformation given by Eq.(1.5), a couple of different schemes for handling the meson mass M_0 in Eq.(1.5) have appeared in the literatures [2–12]. While in invariant meson mass scheme [2,6–12], the meson mass square M_0^2 is given by

$$M_0^2 = \frac{\mathbf{k}_\perp^2 + m_q^2}{x} + \frac{\mathbf{k}_\perp^2 + m_{\bar{q}}^2}{1-x}, \quad (1.6)$$

in the spin-averaged meson mass scheme [3–5], M_0 was taken as the average of physical masses with appropriate weighting factors from the spin degrees of freedom. Nevertheless, once the best fit parameters were used [5,9], both schemes provided the predictions that were not only pretty similar with each other but also remarkably good [5,7] compared to the available experimental data [17] for form factors, decay constants, charge radii *etc.* of various light pseudoscalar(π, K, η, η') and vector(ρ, K^*, ω, ϕ) mesons as well as their radiative decay widths. The main difference in the best fit parameters was the constituent quark masses, *i.e.*, $m_u = m_d = 330$ MeV, $m_s = 450$ MeV in the spin-averaged meson mass scheme [3–5] while $m_u = m_d = 250$ MeV, $m_s = 370$ MeV in the invariant meson mass scheme [7].

Also, among the literatures [7,8,10] using the invariant meson mass scheme, some literatures [7,8] used the Jacobi factor \mathcal{J} in Eq.(1.2) while some [10] did not. However, we have recently observed [9] that the numerical results of various physical observables from Refs. [7,8] were almost equivalent to those of Ref. [10] regardless of the presence-absence of the Jacobi factor if the same form of radial wave function(*e.g.* Gaussian) was chosen and the best fit model parameters in the radial wave function were used.

However, the effect from the difference in the choice of radial wave function, *e.g.*, harmonic oscillator wave function [7,8,10] versus power-law wave function [11], was so substantial that one could not get the similar result by simply changing the model parameters in the chosen radial wave function. For example, in the phenomenology of various meson radiative decays at low Q^2 , we observed [9] that the gaussian type wave function was clearly better than the power-law wave function in comparison with the available experimental data. On the other hand, the radial function so far has been mostly taken as a model wave function rather than as a solution of QCD motivated dynamical equation. Even though the authors in Ref. [12] adopted the quark potential model developed by Godfrey and Isgur [1] to reproduce the meson mass spectra, their model predictions included neither the mixing angles of $\omega - \phi$ and $\eta - \eta'$ nor the form factors for various radiative decay processes of pseudoscalar and vector mesons.

Thus, in this paper, we attempt to fill this gap between the model wave function and the QCD motivated potential. A gaussian radial wave function is used as a trial function of the variational principle for a QCD motivated Hamiltonian which includes not only the Coulomb plus harmonic oscillator potential but also the hyperfine interaction to obtain the correct $\rho - \pi$

splitting. Accordingly, our analysis covers the mass spectra of light pseudoscalar(π, K, η, η') and vector(ρ, K^*, ω, ϕ) mesons and the mixing angles of $\omega - \phi$ and $\eta - \eta'$ as well as other observables such as charge radii, decay constants, radiative decay widths *etc..* We exploit the invariant meson mass scheme in this model. We also adopt the parametrization to incorporate the quark-annihilation diagrams [18–20] mediated by gluon exchanges and the SU(3) symmetry breaking, *i.e.*, $m_{u(d)} \neq m_s$, in the determination of meson mixing angles.

The paper is organized as follows: In Sec.II, we set up a simple QCD motivated effective Hamiltonian and use the variational principle to find the optimum values of the model parameters, quark masses($m_{u(d)}, m_s$) and gaussian parameters($\beta_{u\bar{u}} = \beta_{u\bar{d}} = \beta_{d\bar{d}}, \beta_{u\bar{s}}, \beta_{s\bar{s}}$). In Sec.III, we analyze the meson mass spectra and predict the mixing angles of $\omega - \phi$ and $\eta - \eta'$. We adopt the formulation to incorporate the quark-annihilation diagrams and the effect of SU(3) symmetry breaking in the meson mixing angles. In Sec.IV, we calculate the decay constants, charge radii, form factors and radiative decay rates of various light pseudoscalar and vector mesons and discuss the numerical results in comparison with the available experimental data. Summary and discussions follow in Sec.V.

II. A QCD MOTIVATED HAMILTONIAN AND VARIATIONAL PRINCIPLE

The QCD motivated effective Hamiltonian for the description of the meson mass spectra is given by [1,12]

$$H_{q\bar{q}} = H_0 + V_{q\bar{q}} = \sqrt{m_q^2 + k^2} + \sqrt{m_{\bar{q}}^2 + k^2} + V_{q\bar{q}} \quad (2.1)$$

where $m_q(m_{\bar{q}})$ is the constituent quark(anti-quark) mass and $k^2 = \mathbf{k}_\perp^2 + k_n^2$. In this work, we use the interaction potential $V_{q\bar{q}}$ for the pseudoscalar(0^{-+}) and vector(1^{--}) mesons including not only the Coulomb plus harmonic oscillator confining potential but also the hyperfine interaction which is essential to distinguish vector from pseudoscalar mesons:

$$\begin{aligned} V_{q\bar{q}} &= V_0(r) + V_{\text{hyp}}(r) \\ &= a + br^2 - \frac{4\kappa}{3r} + \frac{2\vec{S}_q \cdot \vec{S}_{\bar{q}}}{3m_q m_{\bar{q}}} \nabla^2 V_{\text{Coul}}, \end{aligned} \quad (2.2)$$

where $\nabla^2 V_{\text{Coul}} = 16\pi\kappa\delta^3(r)/3$ and

$$\langle \vec{S}_q \cdot \vec{S}_{\bar{q}} \rangle = \begin{cases} 1/4 & \text{for vector} \\ -3/4 & \text{for pseudoscalar.} \end{cases} \quad (2.3)$$

As we mentioned in the introduction, we use the gaussian radial wave function of our light-cone quark model as a trial function of the variational principle

$$\phi(x, \mathbf{k}_\perp) = \left(\frac{1}{\pi^{3/2} \beta^3} \right)^{1/2} \exp(-k^2/2\beta^2), \quad (2.4)$$

where $\phi(x, \mathbf{k}_\perp)$ is normalized according to

$$\sum_{\nu\bar{\nu}} \int_0^1 dx \int d^2\mathbf{k}_\perp |\Psi(x, \mathbf{k}_\perp, \nu\bar{\nu})|^2 = \int_0^1 \mathcal{J} dx \int d^2\mathbf{k}_\perp |\phi(x, \mathbf{k}_\perp)|^2 = 1. \quad (2.5)$$

We think that this trial function given by Eq.(2.4) is an effective choice because not only Eq.(2.4) takes the same form as the ground state solution of the harmonic oscillator potential but also it is consistent with the light-cone quark model wave function which has been quite successful in describing various meson properties [3–10]. Furthermore, as we will show below after fixing the parameters a, b and κ , our effective potential $V_0(r)$ turns out to be very similar in the relevant range of potential($r \lesssim 2$ fm) to the usual Coulomb plus linear confining potential(see Fig.1) which is frequently used in the literatures [1,12,21–25].

We now discuss how to fix the parameters of our model, *i.e.*, quark masses(m_u, m_s), gaussian parameters($\beta_{u\bar{u}} = \beta_{u\bar{d}}, \beta_{u\bar{s}}, \beta_{s\bar{s}}$) and potential parameters (a, b, κ) in $V_{q\bar{q}}$ given by Eq.(2.2). Since all the higher order perturbative contributions from the hyperfine interaction $V_{\text{hyp}}(r)$ in Eq.(2.2) vanishes in our calculations of mass spectra for the ground states of pseudoscalar and vector mesons, we can separate $V_{\text{hyp}}(r)$ from our variational calculation and treat it as the first order perturbation. This approach has an advantage of not discriminating the gaussian parameter set $\beta = (\beta_{u\bar{u}}, \beta_{u\bar{s}}, \beta_{s\bar{s}})$ by the spin structure of mesons. Thus, using the variational principle for the spin-independent part of $H_{q\bar{q}}$ in Eq.(2.1),

$$\frac{\partial \langle H_0 + V_0 \rangle}{\partial \beta} = 0, \quad (2.6)$$

we obtain

$$b = \frac{\beta^3}{3} \left\{ \frac{\partial \langle M_0 \rangle}{\partial \beta} - \frac{8\kappa}{3\sqrt{\pi}} \right\}, \quad (2.7)$$

where $\langle H_0 \rangle = \langle M_0 \rangle = \langle \phi(x, \mathbf{k}_\perp) | M_0 | \phi(x, \mathbf{k}_\perp) \rangle$. Eq.(2.7) implies that the variational principle reduces a degree of freedom in the parameter space by expressing b in terms of κ or vice versa. Calculating the expectation value of $H_{q\bar{q}}$ given by Eq.(2.1), we find the optimized values of the model parameters in accordance with the variational principle in Eq.(2.7). We first take the parameters of $m_{u(d)} = 0.25$ GeV and $\beta_{u\bar{u}} = 0.3194$ GeV from Ref. [7] because these values of $m_{u(d)}$ and $\beta_{u\bar{u}}$ have been quite successful in describing various observables of

π and ρ mesons [7]. Using Eq.(2.7) and $(m_u, \beta_{u\bar{u}})$, we then obtain the parameters (a, b, κ) as follows by fitting the correct $\rho - \pi$ mass splitting, *i.e.*, $\langle H_{u\bar{u}}^{V(P)} \rangle = M_{u\bar{u}}^{V(P)} = m_{\rho(\pi)}(P = \text{Pseudoscalar and } V = \text{Vector})$ in Eq.(2.1);

$$a = -0.144 \text{ GeV}, \quad b = 0.010 \text{ GeV}^3, \quad \kappa = 0.607. \quad (2.8)$$

As shown in Fig.1, it is interesting to note that our Coulomb plus harmonic oscillator potential $V_0(r)$ with these values of a, b , and κ in Eq.(2.8) is quite comparable to the Coulomb plus linear quark potential model, $V_0(r) = a_l + b_l r - 4\kappa_l/3r$, suggested by Isgur-Scora-Grinstein-Wise(ISGW) [24] and Scora-Isgur(ISGW2) [25]. The range of agreement extends up to $r \sim 2$ fm.

Next, among various sets of $\{m_s, \beta_{u\bar{s}}\}$ satisfying Eq.(2.7), we find $m_s = 0.48$ GeV and $\beta_{u\bar{s}} = 0.3419$ GeV by fitting optimally the masses of K^* and K , *i.e.*, $M_{u\bar{s}}^{V(P)} = m_{K^*(K)}$. Once the set of $\{m_s, \beta_{u\bar{s}}\}$ is fixed, then the parameter $\beta_{s\bar{s}} = 0.3681$ GeV can be obtained from Eq.(2.7). These optimized model parameters are summarized in Table I. In fixing all of these parameters, the variational principle given by Eq.(2.7) plays the crucial role for $u\bar{u}, u\bar{s}$, and $s\bar{s}$ meson systems to share the same potential parameters (a, b, κ) regardless of their quark-antiquark contents. Subsequently, $M_{s\bar{s}}^V$ and $M_{s\bar{s}}^P$ are predicted as 996 MeV and 732 MeV, respectively. As shown in Fig.2, the solid, dotted and dot-dashed lines are fixed by the parameter sets of $\{m_u, \beta_{u\bar{u}}\}$, $\{m_s, \beta_{u\bar{s}}\}$, and $\beta_{s\bar{s}}$, respectively, and these three lines cross the same point in the space of b and κ if the parameters in Table I are used. The determination of mixing angles and mass spectra of (ω, ϕ) and (η, η') is presented in the following section.

III. MASS SPECTRA AND MIXING ANGLES OF (ω, ϕ) AND (η, η')

Identifying $(f_1, f_2) = (\phi, \omega)$ and (η, η') for vector and pseudoscalar nonets, the physical meson states f_1 and f_2 are given by

$$\begin{aligned} |f_1\rangle &= -\sin\delta|n\bar{n}\rangle - \cos\delta|s\bar{s}\rangle, \\ |f_2\rangle &= \cos\delta|n\bar{n}\rangle - \sin\delta|s\bar{s}\rangle, \end{aligned} \quad (3.1)$$

where $|n\bar{n}\rangle \equiv 1/\sqrt{2}|u\bar{u} + d\bar{d}\rangle$ and $\delta = \theta_{SU(3)} - 35.26^\circ$ is the mixing angle. These combinations satisfy the (mass)² eigenvalue equation

$$\mathcal{M}^2|f_i\rangle = M_{f_i}^2|f_i\rangle \quad (i = 1, 2). \quad (3.2)$$

Taking into account SU(3) symmetry breaking, we use the following parametrization for \mathcal{M}^2 suggested by Scadron [20]

$$\mathcal{M}^2 = \begin{pmatrix} M_{n\bar{n}}^2 + 2\lambda & \sqrt{2}\lambda X \\ \sqrt{2}\lambda X & M_{s\bar{s}}^2 + \lambda X^2 \end{pmatrix}. \quad (3.3)$$

The parameter λ characterizes the strength of the quark-annihilation graph which couples the $I=0$ $u\bar{u}$ state to $I=0$ $u\bar{u}, d\bar{d}, s\bar{s}$ states with equal strength in the exact SU(3) limit. The parameter X , however, pertains to SU(3) symmetry breaking such that the quark-annihilation graph factors into its flavor parts, with λ , λX and λX^2 representing $u\bar{u} \rightarrow u\bar{u}(d\bar{d})$, $u\bar{u} \rightarrow s\bar{s}$ (or $s\bar{s} \rightarrow u\bar{u}$), and $s\bar{s} \rightarrow s\bar{s}$, respectively. Of course, $X \rightarrow 1$ in the SU(3) limit. Also, in Eq.(3.3), $M_{n\bar{n}}^2$ and $M_{s\bar{s}}^2$ describe the masses of the corresponding mesons in the absence of mixing.

Solving Eqs.(3.1)-(3.3), we obtain [20]

$$\tan^2 \delta = \frac{(M_{f_2}^2 - M_{n\bar{n}}^2)(M_{s\bar{s}}^2 - M_{f_1}^2)}{(M_{f_2}^2 - M_{s\bar{s}}^2)(M_{f_1}^2 - M_{n\bar{n}}^2)}, \quad (3.4)$$

$$\lambda = \frac{(M_{f_1}^2 - M_{n\bar{n}}^2)(M_{f_2}^2 - M_{n\bar{n}}^2)}{2(M_{s\bar{s}}^2 - M_{n\bar{n}}^2)}, \quad (3.5)$$

$$X^2 = \frac{2(M_{f_2}^2 - M_{s\bar{s}}^2)(M_{s\bar{s}}^2 - M_{f_1}^2)}{(M_{f_2}^2 - M_{n\bar{n}}^2)(M_{f_1}^2 - M_{n\bar{n}}^2)}, \quad (3.6)$$

and

$$\tan 2\delta = \frac{2\sqrt{2}\lambda X}{(M_{s\bar{s}}^2 - M_{n\bar{n}}^2 + \lambda X^2 - 2\lambda)}, \quad (3.7)$$

which are the model independent equations for any meson $q\bar{q}$ nonets. The Eqs.(3.5) and (3.6) are identical to the two constraints, $\text{Tr}(\mathcal{M}^2) = \text{Tr}(M_{f_i}^2)$ and $\det(\mathcal{M}^2) = \det(M_{f_i}^2)$. The sign of δ is fixed by the signs of the λ and X from Eq.(3.7). Also, since Eq.(3.3) is decoupled from the subspace of $(u\bar{u} - d\bar{d})/\sqrt{2}$, the physical masses of m_π and m_ρ are confirmed to be the masses of $M_{n\bar{n}}^P$ and $M_{n\bar{n}}^V$, respectively, as we used in Sec.II to fix the parameters (a, b, κ) .

Given the fixed physical masses of $M_{n\bar{n}}^P = m_\pi$ and $M_{n\bar{n}}^P = m_\rho$ together with M_{f_i} ($i = 1, 2$), the magnitudes of mixing angles for $\eta - \eta'$ and $\omega - \phi$ now depend only on the masses of $M_{s\bar{s}}^P$ and $M_{s\bar{s}}^V$, respectively, from Eq.(3.4). However, from Eqs.(3.5)-(3.7), one can see that the sign of mixing angle depends on the sign of parameter X . While $X_P > 0$ is well supported by the particle data group [17] ($-23^\circ \lesssim \theta_{SU(3)}^{\eta-\eta'} \lesssim -10^\circ$), the sign of X_V is not yet definite at the present stage of phenomenology. Regarding on the sign of mixing angle δ_V , it is interesting to note that $X_V < 0$ is required for phenomenological fitting of $\delta_V \approx -3.3^\circ (= \theta_{SU(3)} - 35.26^\circ)$

presented in Ref. [7], which has also been suggested by Refs. [26,27] in favor of the current-mixing model [28]. On the other hand, the conventional Gell-Mann-Okubo mass formula for the exact SU(3) limit($X \rightarrow 1$) predicts $\delta_V \approx 0^\circ$ in the linear mass scheme and $\delta_V \approx +3.3^\circ$ in the quadratic mass scheme [17].

In order to predict the $\omega - \phi$ and $\eta - \eta'$ mixing angles, we use the physical masses [17] of $M_{f_1} = (m_\phi, m_\eta)$ and $M_{f_2} = (m_\omega, m_{\eta'})$ as well as the masses of $M_{ss}^V = 996$ MeV and $M_{ss}^P = 732$ MeV determined in Sec.II. Our predictions for $\omega - \phi$ and $\eta - \eta'$ mixing angles are $|\delta_V| \approx 4.2^\circ$ and $\theta_{SU(3)} \approx -19.3^\circ$, respectively. The used mass spectra of light pseudoscalar and vector mesons are summarized in Table II. As discussed above, we will keep both signs of δ_V in $\omega - \phi$ mixing case when we compare various physical observables in the next section. The corresponding results of the mixing parameters $\lambda_{V(P)}$ and $X_{V(P)}$ in Eqs.(3.5) and (3.6) are given by

$$\begin{aligned} \lambda_V &= 0.57m_\pi^2 \text{ GeV}^2, & X_V &= \pm 2.10, \\ \lambda_P &= 13.5m_\pi^2 \text{ GeV}^2, & X_P &= 0.84. \end{aligned} \quad (3.8)$$

Here, $X_V = \pm 2.10$ corresponds to $\delta_V = \pm 4.2^\circ$, respectively. Our values of λ_V and λ_P are not much different from the predictions of Ref. [20]. The reason why λ_V is much smaller than λ_P , *i.e.*, $\lambda_P \approx 23\lambda_V$ in our calculation and $\lambda_P \approx 18\lambda_V$ in Ref. [20], may be attributed to the fact that in the quark-annihilation graph, the 1^{--} annihilation graph involves one more gluon compared to the 0^{-+} annihilation graph. This also indicates the strong departure of $\eta - \eta'$ from the ideal mixing.

IV. APPLICATION

In this section, we now use the optimum model parameters determined in the last two sections and calculate various physical observables; (1) decay constants of light pseudoscalar and vector mesons, (2) charge radii of pion and kaon, (3) form factors of neutral and charged kaons, and (4) radiative decay widths for the $V(P) \rightarrow P(V)\gamma$ and $P \rightarrow \gamma\gamma$ transitions.

Our calculation is carried out using the standard light-cone frame($q^+ = q^0 + q^3 = 0$) with $\mathbf{q}_\perp^2 = Q^2 = -q^2$. The charge form factor of the pseudoscalar meson can be expressed for the ‘+’-component of the current J^μ as follows

$$F(Q^2) = e_q I(Q^2, m_q, m_{\bar{q}}) + e_{\bar{q}} I(Q^2, m_{\bar{q}}, m_q), \quad (4.1)$$

where $e_q (e_{\bar{q}})$ is the charge of quark(anti-quark) and

$$I(Q^2, m_q, m_{\bar{q}}) = \int_0^1 dx \int d^2 \mathbf{k}_\perp \sqrt{\mathcal{J} \mathcal{J}'} \phi(x, \mathbf{k}_\perp) \phi^*(x, \mathbf{k}'_\perp) \frac{\mathcal{A}^2 + \mathbf{k}_\perp \cdot \mathbf{k}'_\perp}{\sqrt{\mathcal{A}^2 + \mathbf{k}_\perp^2} \sqrt{\mathcal{A}^2 + \mathbf{k}'_\perp^2}}, \quad (4.2)$$

with the definition of \mathcal{A} and \mathbf{k}'_\perp given by

$$\mathcal{A} = xm_{\bar{q}} + (1-x)m_q, \quad \mathbf{k}'_\perp = \mathbf{k}_\perp + (1-x)\mathbf{q}_\perp. \quad (4.3)$$

Subsequently, the charge radius of the meson can be calculated by $r^2 = -6dF(Q^2)/dQ^2|_{Q^2=0}$. Also, the decay constant f_P of the pseudoscalar meson ($P = \pi, K$) is given by

$$f_P = \frac{\sqrt{6}}{(2\pi)^{3/2}} \int_0^1 dx \int d^2 \mathbf{k}_\perp \sqrt{\mathcal{J}} \phi(x, \mathbf{k}_\perp) \frac{\mathcal{A}}{\sqrt{\mathcal{A} + \mathbf{k}_\perp^2}}. \quad (4.4)$$

Since all other formulae for the physical observables such as the vector meson decay constants f_V of $V \rightarrow e^+e^-$, decay rates for the $V(P) \rightarrow P(V)\gamma$ and $P \rightarrow \gamma\gamma$ transitions have already been given in our previous publication [5] and also in other references(*e.g.* Ref. [7]), we do not list them here again. The readers are recommended to look at Refs. [5] and [7] for the details of unlisted formulae. In Fig.3, we show our numerical results for the charge form factors of the charged and neutral kaons and compare with the results of vector model dominance(VMD) [29], where a simple two-pole model of the kaon form factors was assumed, *i.e.*, $F_{K^+(K^0)}(Q^2) = e_{u(d)}m_\omega^2/(m_\omega^2 + Q^2) + e_{s(\bar{s})}m_\phi^2/(m_\phi^2 + Q^2)$. Since our model parameters of $m_u = 0.25$ GeV and $\beta_{u\bar{u}} = 0.3194$ GeV are same with the ones used in Refs. [7] and [11], our numerical result of the pion charge form factor is identical with the Fig.2(solid line) in Ref. [11], which is in an excellent agreement with the available experimental data up to $Q^2 \sim 8$ GeV² region. The decay constants and charge radii of various pseudoscalar and vector mesons for two different $\omega - \phi$ mixing angles $|\delta_V| = 3.3^\circ \pm 1^\circ$ are given in Table III and compared with experimental data [17,30]. Even though our optimal predictions of δ_V was $|\delta_V| = 4.2^\circ$, we varied δ_V value somewhat(*i.e.*, $|\delta_V| = 3.3^\circ \pm 1^\circ$) in Table III to show the sensitivity. The decay widths of the $V(P) \rightarrow P(V)\gamma$ transitions are also given for two different values of δ_V in Table IV. Although it is not easy to see which sign of δ_V is more favorable to the experimental data, the positive sign of δ_V looks a little better than the negative one for the processes of $\omega(\phi) \rightarrow \eta\gamma$ and $\eta' \rightarrow \omega\gamma$ transitions. More observables should be compared with the data in order to give more definite answer for this sign issue of $\omega - \phi$ mixing angle. In Table V, we show the results of $P(= \pi, \eta, \eta') \rightarrow \gamma\gamma$ decay widths obtained from our model with the axial anomaly plus partial conservation of the axial current(PCAC) relations. The predictions of $\eta(\eta') \rightarrow \gamma\gamma$ decay widths using

PCAC are in a good agreement with the data for our $\eta - \eta'$ mixing angle, $\theta_{SU(3)} = -19^\circ$. The predictions of the decay constants for the octet and singlet mesons, *i.e.*, η_8 and η_0 , are $f_8/f_\pi = 1.254$ and $f_0/f_\pi = 1.127$ MeV, respectively. Our predictions of f_8 and f_0 are not much different from the predictions of chiral perturbation theory [31] reported as $f_8/f_\pi = 1.25$ and $f_0/f_\pi = 1.04 \pm 0.04$, respectively. Another important mixing-independent quantity related to f_8 and f_0 is the R -ratio defined by

$$R \equiv \left[\frac{\Gamma(\eta \rightarrow \gamma\gamma)}{m_\eta^3} + \frac{\Gamma(\eta' \rightarrow \gamma\gamma)}{m_{\eta'}^3} \right] \frac{m_\pi^3}{\Gamma(\pi \rightarrow \gamma\gamma)} = \frac{1}{3} \left(\frac{f_\pi^2}{f_8^2} + 8 \frac{f_\pi^2}{f_0^2} \right). \quad (4.5)$$

Our prediction, $R = 2.31$, is quite comparable to the available experimental data [32,33], $R_{\text{exp}} = 2.5 \pm 0.5(\text{stat}) \pm 0.5(\text{syst})$. Also, the Q^2 -dependent decay rates $\Gamma_{P\gamma}(Q^2)$ are calculated from the usual one-loop diagram [5,7] and the results are shown in Figs.4-6. Our results are in a remarkably good agreement with the experimental data [34–36] up to $Q^2 \sim 10$ GeV 2 region. We think that the reason why our model is so successful for $P \rightarrow \gamma^*\gamma$ transition form factors is because the Q^2 -dependence($\sim 1/Q^2$) is due to the off-shell quark propagator in the one-loop diagram and there is no angular condition [5] associated with the pseudoscalar meson.

V. SUMMARY AND DISCUSSIONS

In the light-cone quark model approach, we have investigated the mass spectra, mixing angles, and other physical observables of light pseudoscalar and vector mesons using a QCD motivated potential. The variational principle for the effective Hamiltonian is crucial to find the optimum values of the model parameters. After fixing model parameters, we observed that the central potential $V_0(r)$ in our light-cone quark model analysis is close to that of ISGW(ISGW2) [24,25] model. Using the physical masses of (ω, ϕ) and (η, η') , we were able to predict the $\omega - \phi$ and $\eta - \eta'$ mixing angles as $|\delta_V| \approx 4.2^\circ$ and $\theta_{SU(3)} \approx -19.3^\circ$, respectively. We also have checked that the sensitivity of the mass spectra of (ω, ϕ) to $\sim 1^\circ$ variation of δ_V , *i.e.*, from $\delta_V = 4.2^\circ$ to 3.3° , is within 1% error.

With these fixed model parameters, we have computed the observables such as charge radii, decay constants, and radiative decays of $P(V) \rightarrow V(P)\gamma^*$ and $P \rightarrow \gamma\gamma^*$. As summarized in Tables III, IV, and V, our results for these observables are overall in a remarkable agreement with the available experimental data [17]. Furthermore, our result of the R -ratio presented in Eq.(4.5) is in a very good agreement with the experimental data [32,33]. The

Q^2 dependence of $P \rightarrow \gamma\gamma^*$ processes was also compared with the experimental data up to $Q^2 \sim 8$ GeV 2 . The Q^2 -dependence for these processes is basically given by the off-shell quark propagator in the one-loop diagrams. As shown in Figs.4,5, and 6, our results are in an excellent agreement with the experimental data [34–36]. The charged and neutral kaon form factors were also predicted in Fig.3.

While it is not yet clear which sign of $\omega - \phi$ mixing angle should be taken, the overall agreement between our model with the positive sign, *i.e.*, $\delta_V \sim 3.3^\circ$ and the available experimental data seems to be quite good. If we were to choose the sign of X as $X > 0$, then the fact that the mass difference $m_\omega - m_\rho$ is positive is correlated with the sign of the $\omega - \phi$ mixing angle [37]. In other words, $m_\omega > m_\rho$ implies $\delta_V > 0$ from Eqs.(3.5)–(3.7). Perhaps, the precision measurement of $\phi \rightarrow \eta'\gamma$ envisioned in the future at TJNAF experiment might be helpful to give more stringent test of δ_V . In any case, more observables should be compared with the experimental data to give more definite assessment on this sign issue. The extension of the variational method for the effective Hamiltonian to the heavy(b and c quark sector) pseudoscalar and vector mesons and the 0^{++} scalar mesons is in progress.

ACKNOWLEDGMENTS

We are grateful to Prof. Nathan Isgur for his careful reading of this paper and providing useful information on the sign issue of the $\omega - \phi$ mixing. This work was supported by the Department of Energy under DE-FG02-96ER40947. The North Carolina Supercomputing Center and the National Energy Research Scientific Computer Center are also acknowledged for the grant of supercomputer time.

TABLES

TABLE I. Optimized quark masses m_q and the gaussian parameters β obtained from the variational principle. $q=u$ and d .

m_q [GeV]	m_s [GeV]	$\beta_{q\bar{q}}$ [GeV]	$\beta_{s\bar{s}}$ [GeV]	$\beta_{q\bar{s}}$ [GeV]
0.25	0.48	0.3194	0.3681	0.3419

TABLE II. Fit of the ground state meson masses with the parameters given in Table I. The $\omega - \phi$ and $\eta - \eta'$ mixing angles are predicted as $|\delta_V| = 4.2^\circ$ and $\theta_{SU(3)} = \delta_P + 35.25^\circ = -19^\circ$, respectively.

0^{-+}	Experiment[MeV]	Theory	1^{--}	Experiment	Theory
π	135 ± 0.00035	135	ρ	770 ± 0.8	770
K	494 ± 0.016	470	K^*	892 ± 0.24	875
η	547 ± 0.19	547	ω	782 ± 0.12	782
η'	958 ± 0.14	958	ϕ	1020 ± 0.008	1020

TABLE III. Decay constants and charge radii for various pseudoscalar and vector mesons. For comparison, we use two different mixing angles of $\omega - \phi$, $|\delta_V| = 3.3^\circ \pm 1^\circ$. The experimental data are taken from Ref.[17], unless otherwise noted.

Observables	$\delta_V = -3.3^\circ \pm 1^\circ$	$\delta_V = +3.3^\circ \pm 1^\circ$	Experiment
f_π [MeV]	92.4	92.4	92.4 ± 0.25
f_K [MeV]	109.3	109.3	113.4 ± 1.1
f_ρ [MeV]	151.9	151.9	152.8 ± 3.6
f_{K^*} [MeV]	157.6	157.6	—
f_ω [MeV]	45.9 ± 1.4	55.1 ± 1.3	45.9 ± 0.7
f_ϕ [MeV]	82.6 ± 0.8	76.7 ± 1.0	79.1 ± 1.3
r_π^2 [fm 2]	0.449	0.449	0.432 ± 0.016 [30]
$r_{K^+}^2$ [fm 2]	0.384	0.384	0.34 ± 0.05 [30]
$r_{K^0}^2$ [fm 2]	-0.091	-0.091	-0.054 ± 0.101 [30]

TABLE IV. Radiative decay widths for the $V(P) \rightarrow P(V)\gamma$ transitions. The used mixing angles for $\eta - \eta'$ and $\omega - \phi$ are $\theta_{SU(3)} = -19^\circ$ and $|\delta_V| = 3.3^\circ \pm 1^\circ$, respectively. The experimental data are taken from Ref.[17].

Widths	$\delta_V = -3.3^\circ \pm 1^\circ$	$\delta_V = +3.3^\circ \pm 1^\circ$	Experiment[keV]
$\Gamma(\rho^\pm \rightarrow \pi^\pm \gamma)$	76	76	68 ± 8
$\Gamma(\omega \rightarrow \pi\gamma)$	730 ± 1.3	730 ± 1.3	717 ± 51
$\Gamma(\phi \rightarrow \pi\gamma)$	$5.6_{+3.9}^{-2.9}$	$5.6_{-2.9}^{+3.9}$	5.8 ± 0.6
$\Gamma(\rho \rightarrow \eta\gamma)$	59	59	58 ± 10
$\Gamma(\omega \rightarrow \eta\gamma)$	8.7 ± 0.3	6.9 ± 0.3	7.0 ± 1.8
$\Gamma(\phi \rightarrow \eta\gamma)$	38.7 ± 1.6	49.2 ± 1.6	55.8 ± 3.3
$\Gamma(\eta' \rightarrow \rho\gamma)$	67.5	67.5	61 ± 8
$\Gamma(\eta' \rightarrow \omega\gamma)$	4.9 ± 0.4	7.6 ± 0.4	6.1 ± 1.1
$\Gamma(\phi \rightarrow \eta'\gamma)$	0.41 ± 0.007	0.36 ± 0.007	< 1.8
$\Gamma(K^{*0} \rightarrow K^0\gamma)$	124.5	124.5	117 ± 10
$\Gamma(K^{*+} \rightarrow K^+\gamma)$	79.5	79.5	50 ± 5

TABLE V. Radiative decay widths $\Gamma(P \rightarrow \gamma\gamma)$ for $\eta - \eta'$ mixing angle, $\theta_{SU(3)} = -19^\circ$. Our model predictions were obtained by using the axial anomaly plus PCAC relations. The experimental data are taken from Ref.[17].

Widths	Our model with PCAC relations	Experiment
$\Gamma(\pi \rightarrow \gamma\gamma)$	7.73	7.8 ± 0.5 [eV]
$\Gamma(\eta \rightarrow \gamma\gamma)$	0.42	0.47 ± 0.05 [keV]
$\Gamma(\eta' \rightarrow \gamma\gamma)$	4.10	4.3 ± 0.6 [keV]

REFERENCES

- [1] S. Godfrey and N. Isgur, Phys. Rev. D **32**, 189(1985).
- [2] M. V. Terent'ev, Yad. Fiz. **24**, 207(1976) [Sov.J. Nucl. Phys. **24**, 106(1976)]; V. B. Berestetsky and M. V. Terent'ev, *ibid.* **24**, 1044(1976) [**24**, 547(1976)]; **25**, 653(1977)[**25**, 347(1977)].
- [3] Z. Dziembowsky and L. Mankiewicz, Phys. Rev. Lett. **58**, 2175(1987); Z. Dziembowsky, Phys. Rev. D **37**, 778(1988).
- [4] C.-R. Ji and S.R. Cotanch, Phys. Rev. D **41**, 2319(1990); C.-R. Ji, P.L. Chung and S.R. Cotanch, Phys. Rev. D **45**, 4214(1992).
- [5] H.-M. Choi and C.-R.Ji, Nucl. Phys. A **618**, 291(1997).
- [6] W. Jaus, Phys. Rev. D **41**, 3394(1990).
- [7] W. Jaus, Phys. Rev. D **44**, 2851(1991).
- [8] P.L. Chung, F. Coester, and W.N. Polyzou, Phys. Lett. B **205**, 545(1988).
- [9] H.-M. Choi and C.-R.Ji, Phys. Rev. D **56**, 6010(1997).
- [10] T.Huang,B.-Q. Ma, and Q.-X.Shen, Phys.Rev.D **49**, 1490(1994).
- [11] F.Schlumpf, Phys.Rev.D.**50**, 6895(1994).
- [12] F. Cardarelli *et al.*, Phys. Lett. B **349**, 393(1995); **359**, 1(1995).
- [13] C.-R. Ji and S.J. Rey, Phys. Rev. D **53**, 5815(1996).
- [14] Y. Kuramashi *et al.*, Phys. Rev. Lett. **72**, 3448(1994).
- [15] C.-R.Ji and Y.Surya, Phys.Rev. D **46**, 3565(1992).
- [16] D.E.Soper, ph.D. Thesis, SLAC Report No. 137 (1971).
- [17] Particle Data Group, R. M. Barnett *et al.*, Phys. Rev. D **54**, 1(1996).
- [18] A. De Rújula, H. Georgi, and S. Glashow, Phys. Rev. D **12**, 147(1975).
- [19] N. Isgur, Phys. Rev. D **12**, 3770(1975); **13**, 122(1976).
- [20] M. D. Scadron, Phys. Rev. D **29**, 2076(1984).
- [21] W.Lucha, F.F.Schöberl, and D. Gromes, Phys. Rep. **200**, 127(1991).
- [22] N. Isgur and G. Karl, Phys. Lett. B **72**, 109(1977).
- [23] D. Gromes and I. O. Stamatescu, Nucl. Phys. B **112**, 213(1976).
- [24] N. Isgur, D. Scora, B. Grinstein, and M. B. Wise, Phys. Rev. D **39**, 799(1989).
- [25] D. Scora and N. Isgur, Phys. Rev. D **52**, 2783(1992).
- [26] T. Das, V. S. Mathur, and S. Okubo, Phys. Rev. Lett. **19**, 470(1967); J. J. Sakurai, *ibid.* **19**, 803(1967).
- [27] R. J. Oakes and J. J. Sakurai, Phys. Rev. Lett. **19**, 1266(1967).

- [28] S. Coleman and H. J. Schnitzer, Phys. Rev. **134**, B863(1964); N. M. Kroll, T. D. Lee, and B. Zumino, *ibid.* **157**, 1376(1967).
- [29] J. J. Sakurai, K. Schilcher and M. D. Tran, Phys. Lett. B **102**, 55(1981); J. S. Bell and J. Pasupathy, *ibid.* B **83**, 389(1970).
- [30] R. A. Amendolia *et al.*, Phys. Lett. B **178**, 435(1986).
- [31] J. F. Donoghue, B. R. Holstein, and Y. C. R. Lin, Phys. Rev. Lett. **55**, 2766(1985).
- [32] *The second DAΦNE physics handbook*, edited by L. Maiani, G. Pancheri, and N. Paver, published 1995 by INFN-LNF- Divisione Ricerca, ISBN 88-86409-02-8.
- [33] F. Anulli *et al.*, *Measurement of two photon interactions with the KLOE small angle tagging system*, p. 607 in Vol. II of Ref. [32].
- [34] CELLO Collaboration, H.-J. Behrend *et al.*, Z. Phys. C **49**, 401(1991).
- [35] CELLO Collaboration, V. Savinov *et al.*, Report No. hep-ex/9507005.
- [36] TPC/2 γ Collaboration, H. Aihara *et al.*, Phys. Rev. Lett. **64**, 172(1990).
- [37] private communication with Prof. Nathan Isgur.

FIGURES

Fig.1. The variational principle satisfying Eq.(2.7). The solid, dotted, and dot-dashed lines are fixed by the sets of $(m_u, \beta_{u\bar{u}})$, $(m_s, \beta_{u\bar{s}})$, and $(m_s, \beta_{s\bar{s}})$, respectively.

Fig.2. The central potential $V_0(r)$ versus r . Our Coulomb plus harmonic oscillator potential(solid line) compared with the Coulomb plus linear potential of ISGW [24](dotted line) and ISGW2 [25](long-dashed line) models, respectively.

Fig.3. Theoretical predictions of K^+ and K^0 form factors compared with a simple two-pole VMD model [29], $F_{K^+(K^0)}^{\text{VDM}} = e_{u(d)} m_\omega^2 / (m_\omega^2 + Q^2) + e_{\bar{s}} m_\phi^2 / (m_\phi^2 + Q^2)$.

Fig.4. The decay rate for the $\pi \rightarrow \gamma^* \gamma$ transition obtained from the one-loop diagram. Data are taken from Refs. [34,35].

Fig.5. The decay rate for the $\eta \rightarrow \gamma^* \gamma$ transition obtained from the one-loop diagram. Data are taken from Refs. [34–36].

Fig.6. The decay rate for the $\eta' \rightarrow \gamma^* \gamma$ transition obtained from the one-loop diagram. Data are taken from Refs. [34–36].

Fig.1

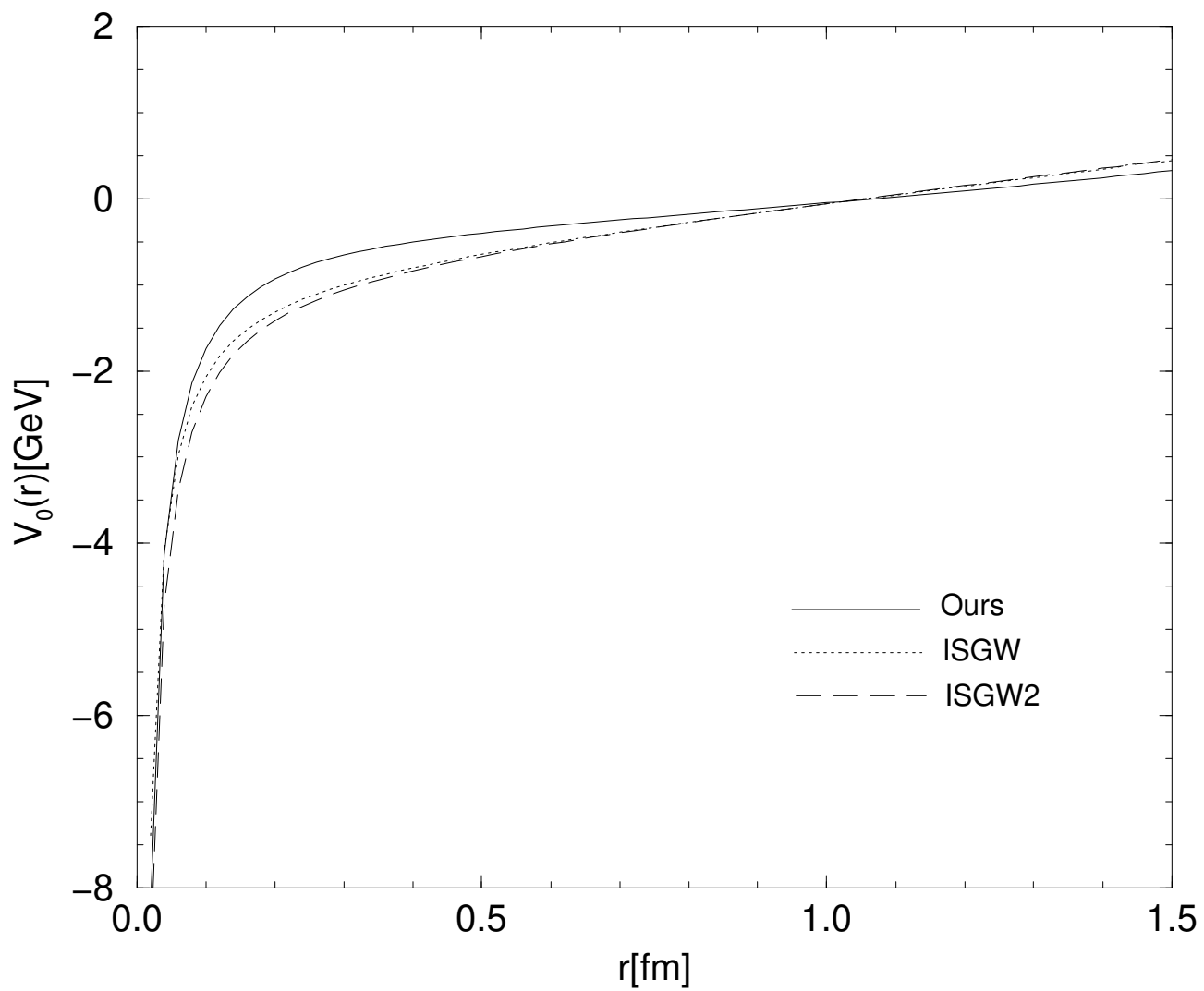


Fig.2

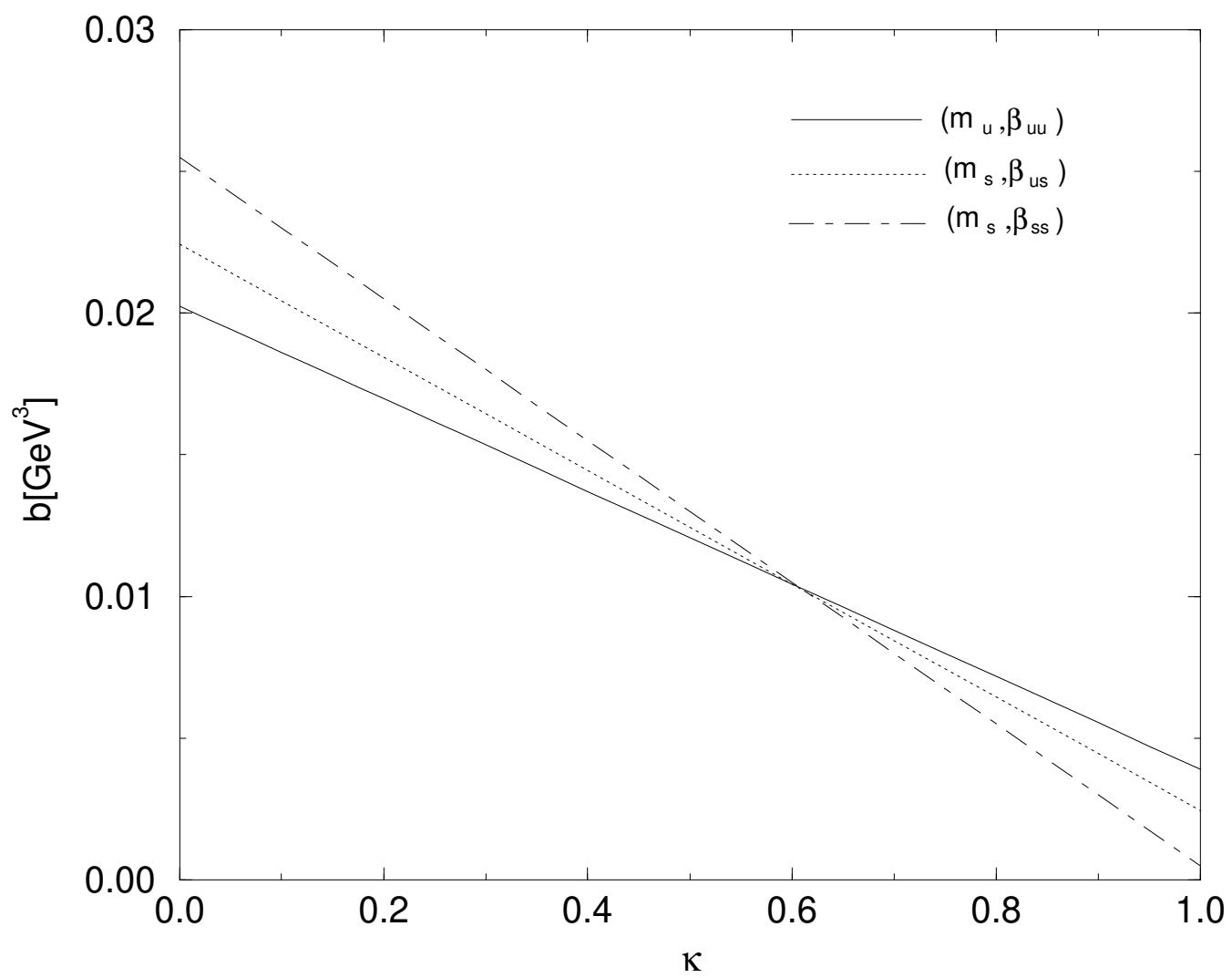


Fig.3

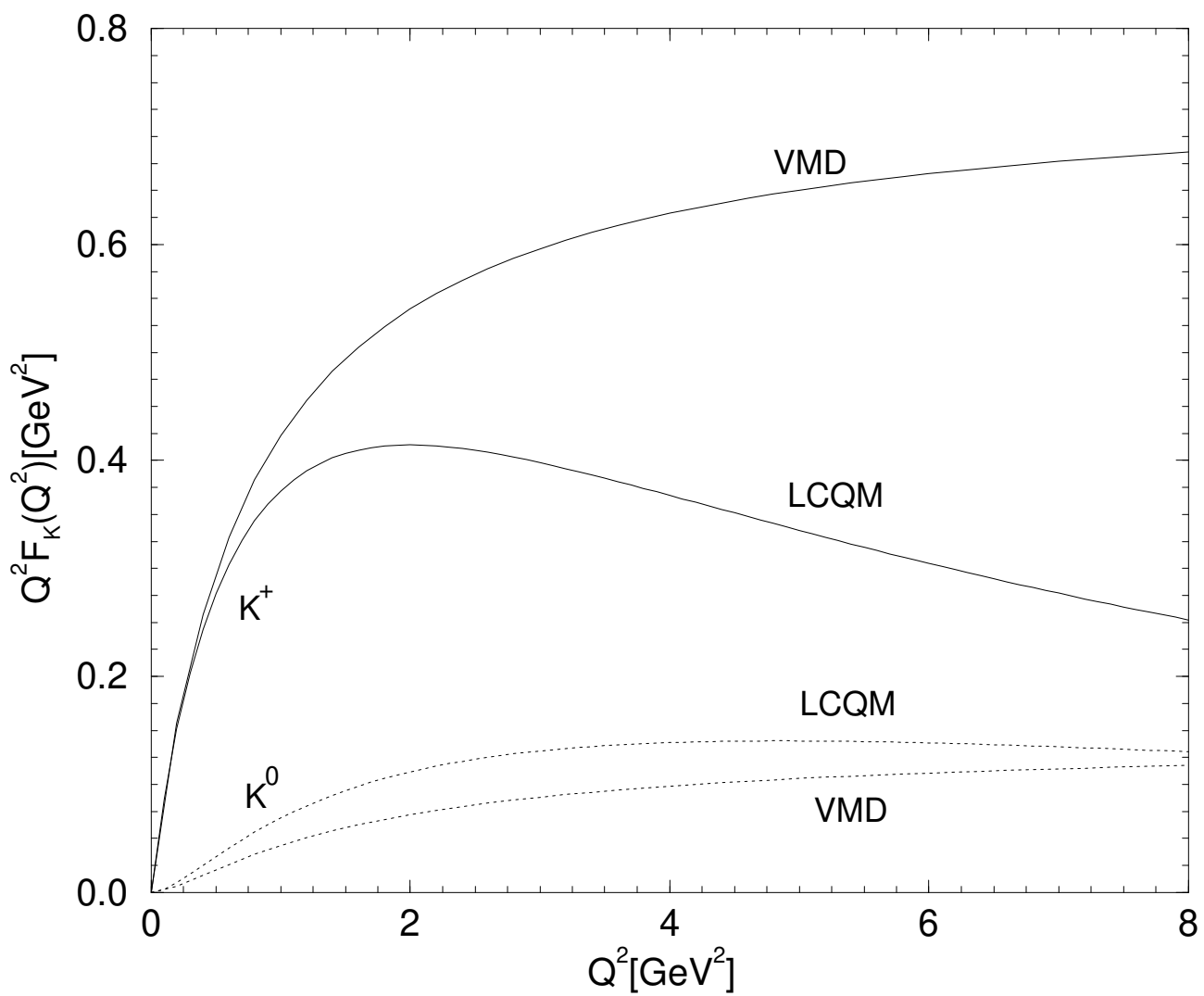


Fig.4

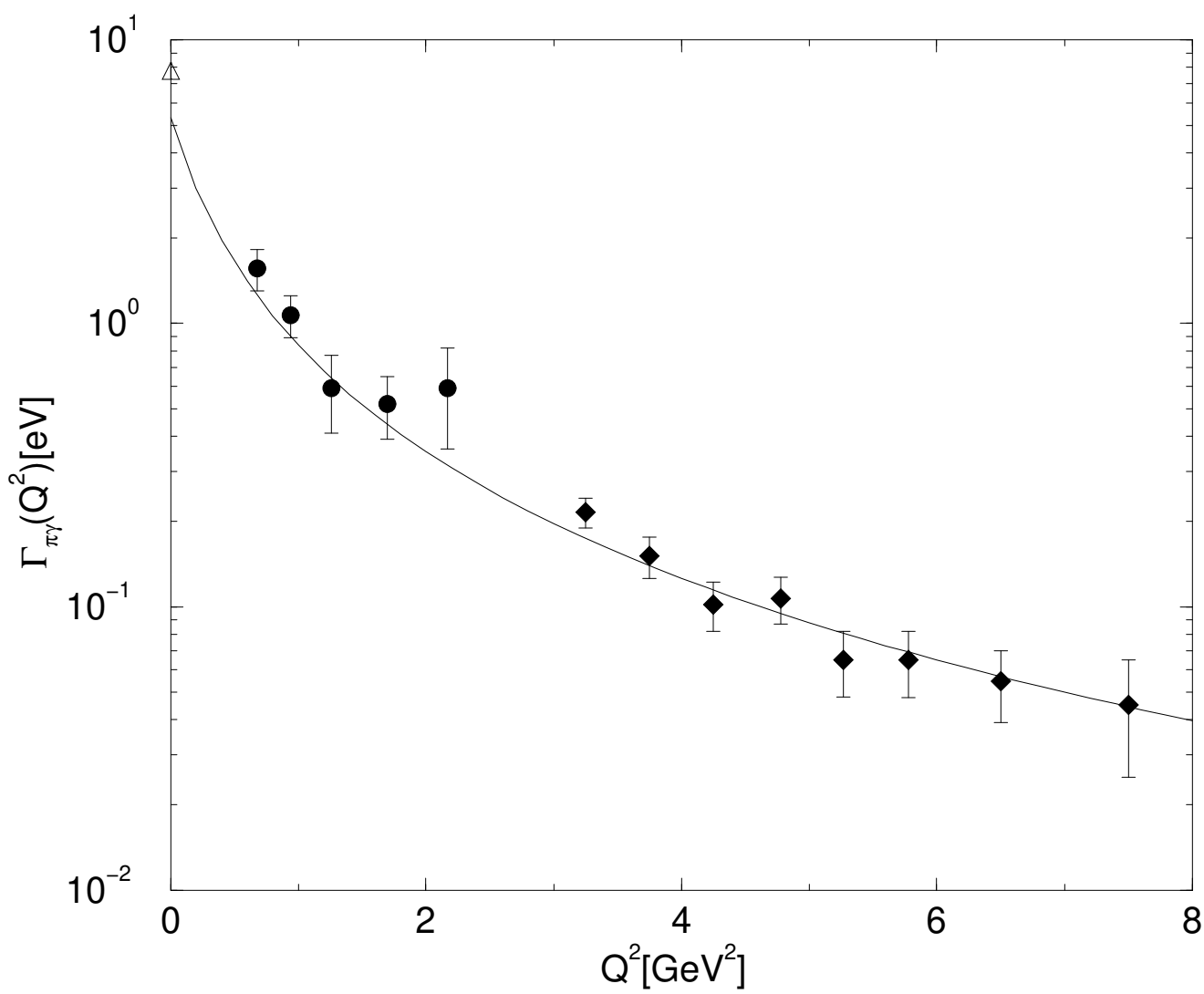


Fig.5

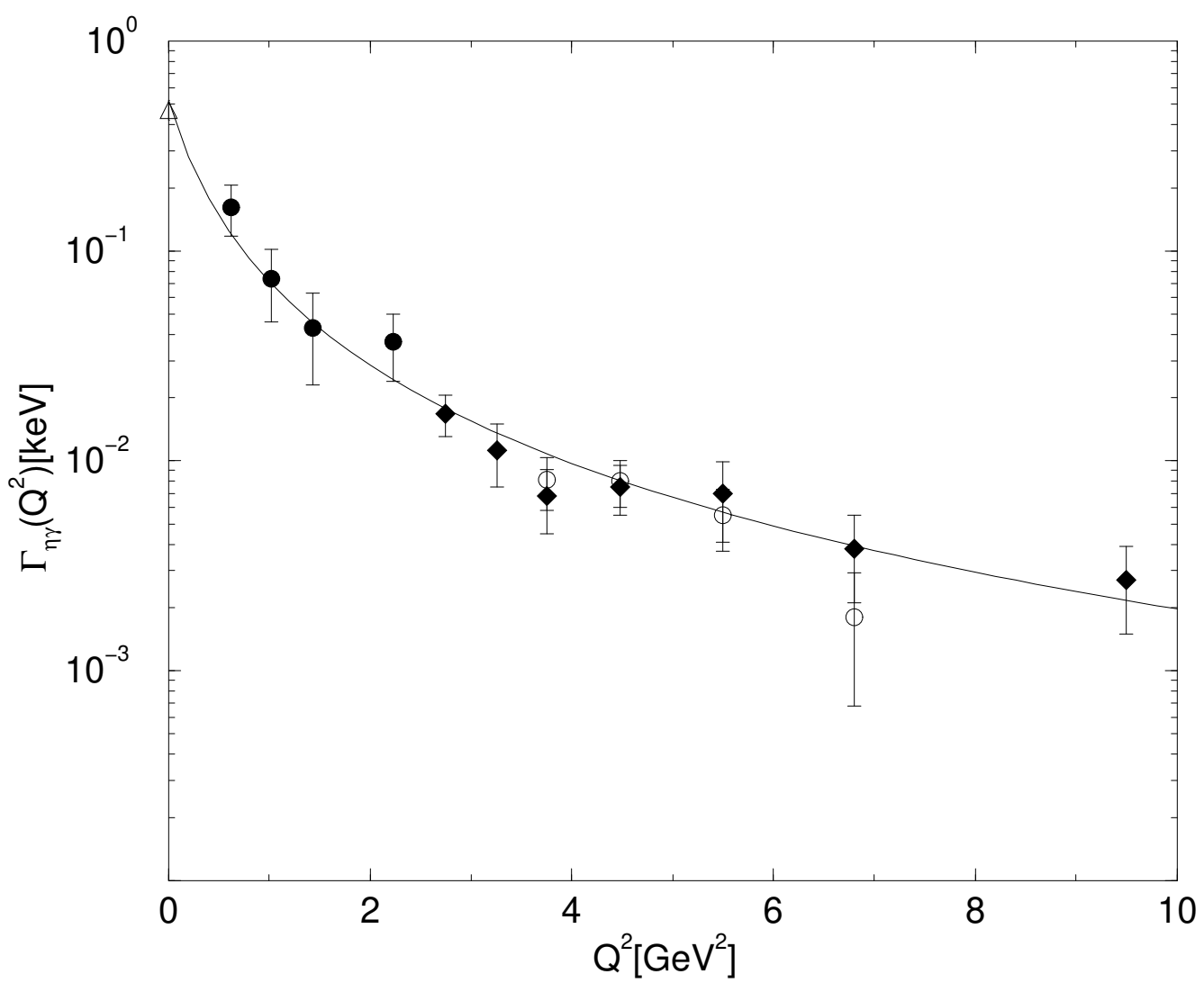


Fig.6

